Electronic Supplementary Information for Chemical Communications

Ion effects on conformation and dynamics of repetitive domain of spider silk protein: Implication on solubility and β-sheet formation

Nur Alia Oktaviani[a], Akimasa Matsugami[b], Fumiaki Hayashi[b] and Keiji Numata*[a]

[a]Biomacromolecules Research Team, RIKEN Center for Sustainable Resource Science, 2-1 Hirosawa, Wako, Saitama 351-0198, Japan

[b]Advanced NMR Application and Platform Team, NMR Research and Collaboration Group, NMR Science and Development Division, RIKEN SPring-8 Center, 1-7-22 Suehiro-cho, Tsurumi-ku, Yokohama, Kanagawa 230-0045 Japan

Corresponding author: Keiji Numata, Email: keiji.numata@riken.jp

Table of Contents

Material and Methods

Fig. S1 Repetitive domains used in this study

Fig. S2 Effect of the chaotropic ion concentrations on the signal intensities of the 15-mer

Fig.S3 Effect of the chaotropic ion concentrations on the signal intensities of the monomer

Fig. S4 Effect of chaotropic ions on the conformation of the repetitive domain (15-mer)

Fig. S5 Normalized VCD intensities of the 15-mer in the absence (red) and presence of 300 mM NaCl (black).

Fig. S6 Effect of chaotropic ions on the dynamics of the repetitive domain (15-mer)

Fig. S7 Complete dynamics measurements of the 15-mer in the presence and absence of 300 mM NaCl

Fig. S8 Spectral density analysis of the 15-mer in the absence and presence of 300 mM NaCl

Fig. S9 Effect of kosmotropic ions (SO_4^{2-}) on the conformation and dynamics of the repetitive domain (15-mer).

Fig. S10 Effect of kosmotropic ions on the amide proton of the repetitive domain

Fig. S11 Higher phosphate concentrations (≥ 600 mM) lead to precipitation of the 15-mer.

Fig. S12 Effect of 300 mM potassium phosphate on the dynamics of the monomer

Fig. S13 Complete dynamics measurements of the 15-mer in the presence of 600 mM potassium phosphate

Fig. S14 Spectral density of the 15-mer in the presence of 600 mM potassium phosphate

Fig. S15 Comparison of J(0) values of the 15-mer in the presence of 600 mM potassium phosphate (black) and in the presence of 300 mM NaCl (red)

References

Material and Methods

Preparation of recombinant silk proteins

The amino acid sequence of the repetitive domain of spidroin was designed based on the consensus repeat (GRGGLGGQGAGAAAAAGGAGQGGYGGLGSQG) of the major ampullate spidroin 1 (MaSp1) sequences from *N. clavipes* (accession code: P19837). The monomer and 15-mer genes, which correspond to 1 and 15 repeat units, respectively, were cloned into the pET30a vector. The repetitive domain was modified with a linker consisting of the restriction sites *Nhe*I and *Spe*I based on a previous report.[1,2]

Recombinant repetitive domains (the 15-mer and monomer) of spidroin were expressed in *E. coli* BL21(DE3) and purified as described previously.[3] For NMR samples, doubly labeled (^{13}C, ^{15}N) repetitive domains (the 15-mer and monomer) were prepared by growing the *E. coli* cells in M9 minimal medium containing 1 g/L ^{15}N-ammnium chloride and 2 g/L ^{13}C-glucose. For the VCD experiment, an unlabeled 15-mer repetitive domain was prepared by expressing the 15-mer in *E. coli* BL21(DE3) using rich Luria Bertani (LB) medium. The NMR samples contained ~0.3 - 0.5 mM recombinant repetitive domain (the 15-mer and monomer) in 10 mM phosphate buffer, pH 7, 10% D_2O and 0.1 mM DSS.

NMR measurements

NMR spectra were recorded using a triple resonance TCI cryogenic probe and a z-axis gradient coil with a Bruker spectrometer (700 MHz). All NMR experiments were conducted at 15°C. Repetitive domains (the 15-mer and monomer) were assigned based on previously deposited BMRB data (accession number 27460). However, due to the differences in the acquisition temperatures, the backbone chemical shift assignments of the 15-mer at 15°C were confirmed using 3D NMR experiments, namely, 3D CBCACONH, 3D HNCA, 3D HNCO and 3D HNCACO. All spectra were processed using NMRPipe[4] and analyzed using NMRFAM-SPARKY.[5] DSS was used as a reference standard for all NMR signals according to IUPAC recommendations.[6] The

structural propensities of the repetitive domain were calculated using the neighbor-corrected structural propensity (ncSPC) calculator.[7]

Different with the previous study[3], the NMR sample conditions in this study were prepared in 3 different conditions, which are in (1) in 10 mM phosphate buffer (2) in the presence of chaotropic ions (Na^+, Ca^{2+}, Mg^{2+} and Cl^-) at different concentrations (3) in the presence of kosmotropic ions (PO_4^{3-}, SO_4^{2-}).

The titration of the chaotropic ions on the repetitive domains (the 15-mer and monomer) was performed at concentrations of 0, 50, 100 and 300 mM NaCl, KCl, $MgCl_2$, and $CaCl_2$. For kosmotropic ions, the repetitive domains were titrated with 0, 50, 100, 300 and 600 mM potassium phosphate and with 0, 50, 100 and 300 mM potassium sulfate. The signal intensity ratios were calculated from the signal intensities from the ^1H-^{15}N HSQC spectra. Each signal was normalized to the intensity of the signals of the alanine residues (residue A13 for the 15-mer or residue A12 for the monomer). The ratio was taken from the normalized signal intensities of the spectra acquired in the presence and absence of chaotropic ions. For each titration point, several 2D NMR experiments, 2D ^1H-^{15}N HSQC, 2D H(N)CO, 2D (H)C(CON)H, and 2D H(CCON)H, were conducted.

The 3D 3J HNHA experiment consisted of 16 scans, a 1 s relaxation delay for every scan, 2048 × 256 × 36 complex points for the $^1H^N$, $^1H\alpha$, and N^H dimensions, respectively, and a spectral width of 16 × 11 × 26 ppm, which correspond to the $^1H^N$, $^1H\alpha$, and N^H dimensions, respectively. The spectrum was collected using nonuniform sampling (50% NUS). All data were processed using NMRPipe[4] and analyzed using NMRFAM-SPARKY.[5] The $^3JHNH\alpha$ coupling constants were calculated based on the intensity ratios of the cross peaks and the diagonal peaks ($I_{cross}/I_{diagonal}$) based on the following equations[8]:

$$I_{cross}/I_{diagonal}=-\tan^2(2\pi^3 J_{HH}\zeta) \quad (1)$$

where ζ is the delay time (13.05 ms) and J_{HH} is the $^{3}J_{HNHA}$ coupling constant.

Complete relaxation experiments ($^{15}NT_1$, $^{15}NT_2$ and {^{1}H}-^{15}N heteronuclear NOE in 2 magnetic fields (700 and 800 MHz)) were performed using ~0.3 mM of (^{13}C, ^{15}N) 15-mer under 3 different conditions:

1. In 10 mM phosphate buffer, pH 7, 10% D_2O and 0.1 mM DSS

2. In 300 mM NaCl, 10 mM phosphate buffer, pH 7, 10% D_2O and 0.1 mM DSS

3. In 600 mM potassium phosphate, pH 7, 10% D_2O and 0.1 mM DSS

Backbone amide ^{15}N transverse (T_2) relaxation experiments of the 15-mer were performed at 15°C on 700 and 800 MHz Bruker spectrometers equipped with a TCI cryogenic probe and a *z*-axis gradient coil. The pulse sequence for ^{1}H-detected $^{15}NT_2$ relaxation recordings led to a series of 2D ^{1}H–^{15}N spectra that were correlated with different $^{15}NT_2$ relaxation delays.[9] The $^{15}NT_2$ relaxation delays were 17, 34, 51, 85, 102, 136, 170, 204 and 238 ms. Each ^{1}H–^{15}N correlation spectrum was acquired using 16 scans, a 1 s relaxation delay, 1024 direct complex points, and 256 indirect complex points. The acquisition times were 45.7 and 70.3 ms for the direct (^{1}H) and indirect (^{15}N) domains, respectively. All data were processed using NMRPipe[4] and analyzed using NMRFAM-SPARKY.[5]

Backbone $^{15}NT_2$ values were determined by fitting the peak intensities using a single-exponential decay:

$$I(t)=I_0\exp(-t/T_2) \qquad (2)$$

where $I(t)$ is the intensity after a delay time t and I_0 is the intensity at time $t = 0$.

Backbone amide ^{15}N longitudinal (T_1) relaxation experiments of the 15-mer were performed at 15°C on 700 and 800 MHz Bruker spectrometers equipped with a TCI cryogenic probe and a *z*-axis gradient coil. The pulse sequence for ^{1}H-detected $^{15}NT_1$ relaxation recordings led to a series of 2D ^{1}H–^{15}N spectra correlated with different $^{15}NT_1$ relaxation delays.[9] The $^{15}NT_1$ relaxation delays were 10, 70, 150, 250, 370, 530, 750, 1150, 1500, 2000, and 2500 ms. Each ^{1}H–^{15}N correlation spectrum was recorded using 16 scans, a 1.6 s relaxation delay, 1024 direct complex points, and 256 indirect complex points. The acquisition times were 45.7 and 70.3 ms for the direct (^{1}H) and indirect (^{15}N) domains, respectively. All data were processed using NMRPipe[4] and analyzed using NMRFAM-SPARKY.[5]

Backbone $^{15}NT_1$ values were determined by fitting the peak intensities using a single-exponential decay, according to the following equation:

$$I(t)=I_0 \exp(-t/T_1) \quad (3)$$

The {^{1}H}-^{15}N steady-state NOE values were recorded by measuring two spectra: an initial spectrum recorded without the initial proton saturation, and a second spectrum recorded with initial proton saturation (3 s). The {^{1}H}–^{15}N steady-state NOE values of the monomer and the 15-mer were determined at 700 and 800 MHz. The steady-state NOE values were calculated based on the ratios of the average intensities of the peaks with and without proton saturation. The standard deviations of the NOE values were calculated from the background noise level using the following formula[10]:

$$\sigma NOE/NOE=((\sigma I_{sat}/I_{sat})^2+(\sigma I_{unsat}/I_{unsat})^2)^{1/2} \quad (4)$$

where I_{sat} and I_{unsat} are the measured intensities of the peaks in the presence and absence of proton saturation, respectively. The noise in the background regions of the spectra, which were

recorded with initial proton saturation and without initial proton saturation, are given by σI_{sat} and σI_{unsat}, respectively.

The amide ^{15}N relaxation was analyzed using a reduced spectral density mapping approach.[11] This method assumes that the spectral density is relatively constant in the high-frequency region near $J(\omega H)$; therefore, $J(\omega H + \omega N) \sim J(\omega H - \omega N) \sim J(0.87\ \omega H)$. The spectral densities at $\omega = \omega N$, $\omega = 0.87\ \omega H$ can be obtained from the following formulas:

$$J(0.87\omega H) = J(\omega H) = \frac{4}{5d^2}\left(\frac{\gamma_N}{\gamma_H}\right)\left(\frac{NOE-1}{T_1}\right) \quad (5)$$

$$J(\omega N) = \frac{\left[\frac{1}{T_1} - \left(\frac{7d^2}{4}\right)J(\omega H)\right]}{\frac{3d^2}{4} + c^2} \quad (6)$$

The spectral densities of $J(0)$ from the two spectrometer frequencies were calculated from the following equations:

$$\mathrm{J}(0) = \frac{1}{\beta}\left[\left\{\frac{1}{T_2^{800}} - \frac{\kappa}{T_2^{700}}\right\} - \frac{3d^2}{8}\{J(\omega_N^{800}) - \kappa J(\omega_N^{700})\} - \frac{c_{800}^2}{2}\{(\omega_N^{800}) - \kappa J(\omega_N^{700})\} - \frac{13d^2}{8}\{J(\omega_H^{800}) - \kappa J(\omega_H^{700})\}\right] \quad (7)$$

$$\text{where } \kappa = \left(\frac{\omega_H^{800}}{\omega_H^{700}}\right)^2 \quad (8)$$

$$\beta = \frac{d^2}{2}(1 - \kappa) \quad (9)$$

$$c = \omega_{\mathrm{N}}(\sigma \parallel - \sigma \perp) \quad (10)$$

$$d = \left(\frac{\mu_0 h}{8\pi^2}\right)\left(\frac{\gamma_{\mathrm{H}}}{\gamma_{\mathrm{N}}}\right)(r_{NH})^{-3}$$

(11)

where h is Planck's constant, μ_0 is the permeability of a vacuum, r_{NH} is the bond length (1.02 Å), $\sigma_{||} - \sigma_{\perp}$ is the axial chemical shift tensors of the backbone ^{15}N nuclei (which are considered to be −160 ppm), and γ_N and γ_H are the gyromagnetic ratios of ^{15}N and ^{1}H, respectively.

VCD measurements

The VCD spectra of the unlabeled 15-mer (2% w/v) in D_2O at neutral pH were measured at room temperature in the absence and presence of 300 mM NaCl. The VCD spectra were measured using a JASCO FVS-6000 system. Baseline corrections were performed by subtracting the spectrum of D_2O. The VCD spectra were acquired in the region of 2000–850 cm^{-1} at a resolution of 4 cm^{-1} and were based on an accumulation of 31992 scans. For comparison, the VCD spectra of the 15-mer both with and without 300 mM NaCl were normalized.

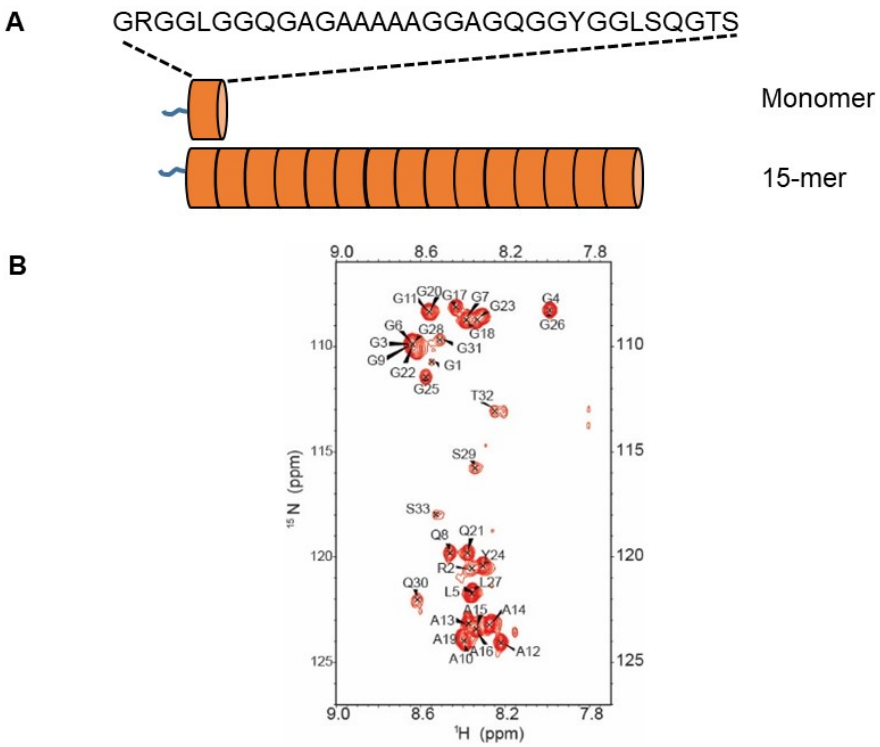

Fig. S1 Repetitive domains used in this study. (A) The amino acid sequence of the recombinant repetitive domains used in this study. The monomer and 15-mer are repetitive domains that contain one and 15 repeat units, respectively. The blue tail indicates a his-tag, which was used to facilitate purification of the repetitive domains. (B) NMR assignment of the 15-mer at 10 mM phosphate buffer, pH 7, at 15°C.

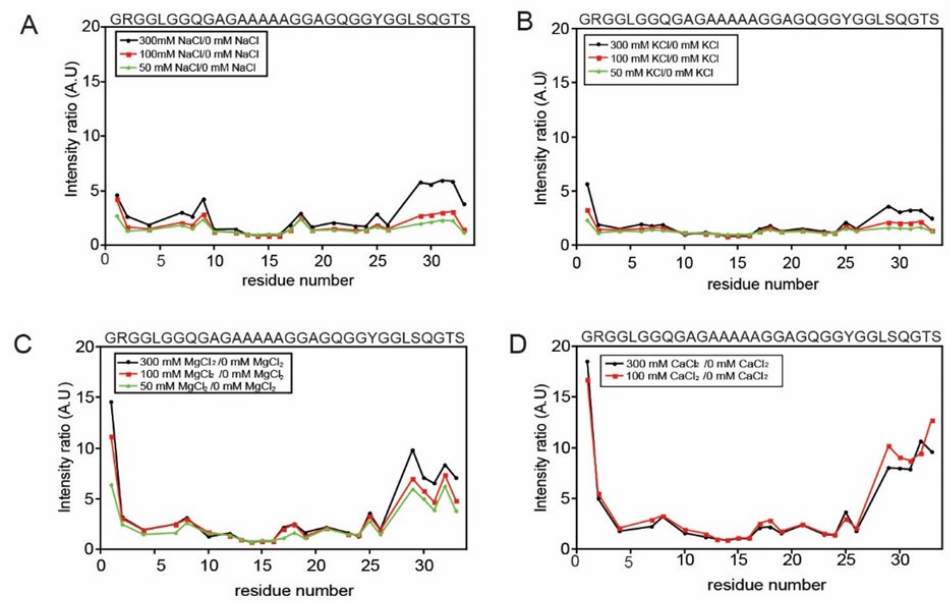

Fig. S2 Effect of the chaotropic ion concentrations on the signal intensities of the 15-mer. (A). The effect of the NaCl concentration on the signal intensities of the 15-mer. (B). The effect of the KCl concentration on the signal intensities of the 15-mer (C). The effect of the $MgCl_2$ concentration on the signal intensities of the 15-mer (D). The effect of the $CaCl_2$ concentration on the signal intensities of the 15-mer. The signal intensity of each residue was taken from the ^{1}H-^{15}N HSQC spectrum of the 15-mer in different chaotropic ion concentrations. All signal intensities were normalized to the intensity of signals of residue A13. The intensity ratio was calculated by taking the ratio of the intensities of the peaks in the presence and absence of chaotropic ions. These results suggest that a higher concentration of chaotropic ions leads to a higher intensity ratio. Chaotropic ions had significant effects on the intensity ratio of the signal of the repetitive domain in the SQGTSG region, while the signal intensities from the polyalanine region (AGAAAAA) were not affected by chaotropic ions.

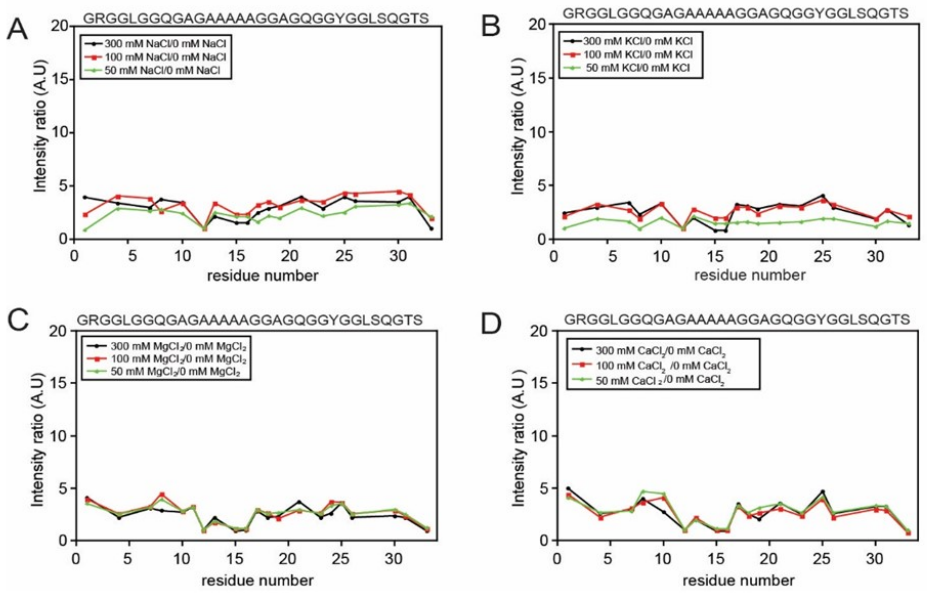

Fig. S3 Effect of the chaotropic ion concentrations on the signal intensities of the monomer. (A). The effect of the NaCl concentration on the signal intensities of the monomer (B). The effect of the KCl concentration on the signal intensities of the monomer (C). The effect of the $MgCl_2$ concentration on the signal intensities of the monomer (D). The effect of the $CaCl_2$ concentration on the signal intensities of the monomer. The signal intensity of each residue was taken from the ^{1}H-^{15}N HSQC spectrum of the monomer at different chaotropic ion concentrations. All signal intensities were normalized to the intensity of the signals from residue A12. Overlapping signals were not considered in this analysis. The intensity ratios were calculated by taking the ratio of the intensity of each signal in the presence and absence of chaotropic ions. Chaotropic ions had a stronger effect of on the intensity ratio of the monomer signals in the glycine-rich region. In contrast to the results of the 15-mer, no dramatic effect was observed on the intensity ratio of the signals from the SQGTSG region of the monomer, which is the chain end of the monomer.

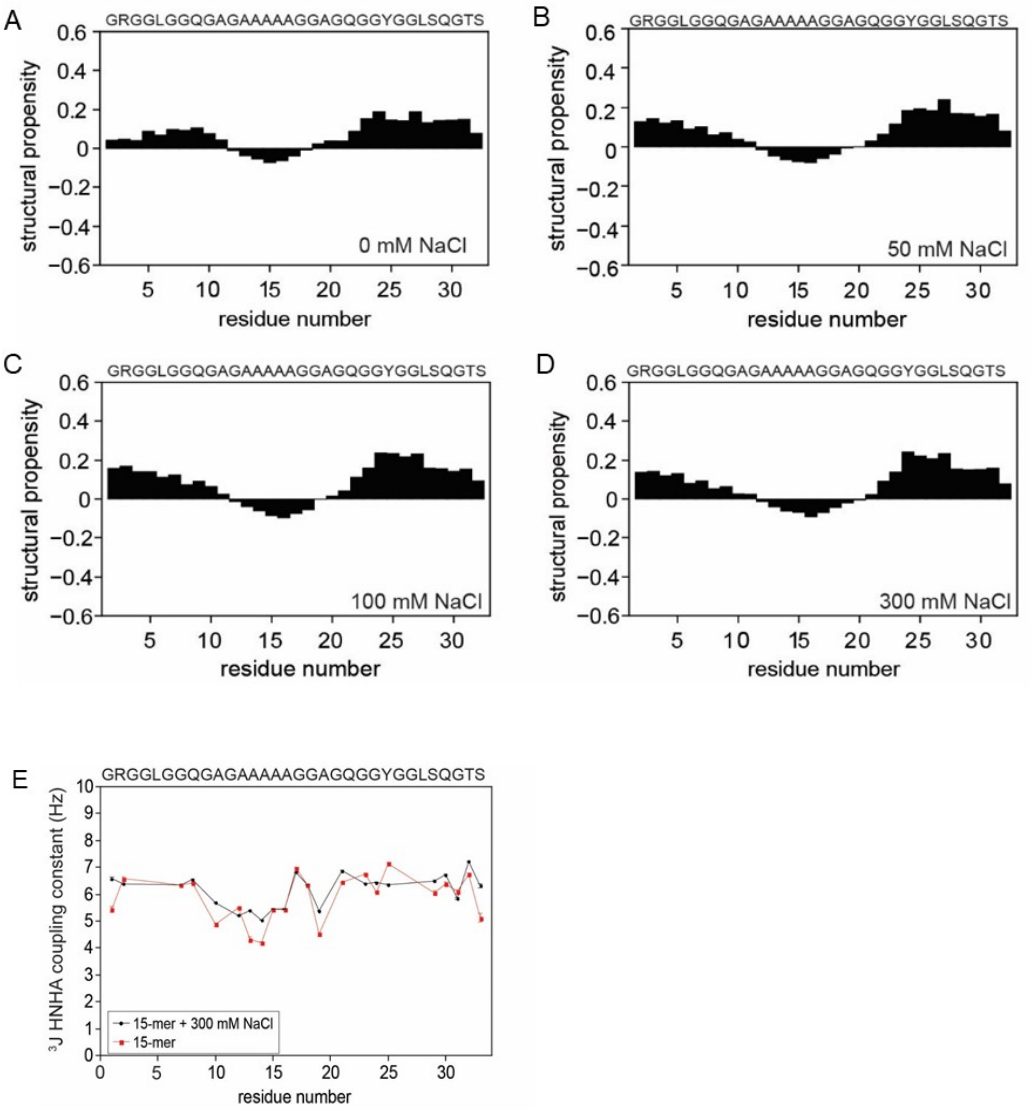

Fig. S4 Effect of chaotropic ions on the conformation of the repetitive domain (15-mer). (A). The effect of 0 mM NaCl on the structural propensity of the 15-mer (B). The effect of 50 mM NaCl on the structural propensity of the 15-mer (C). The effect of 100 mM NaCl on the structural propensity of the 15-mer (D). The effect of 300 mM NaCl on the structural propensity of the 15-mer. Structural propensities were calculated based on the chemical shifts of Cα, Cβ, N^H, CO and Hα using a neighbor-corrected structural propensity calculator (ncSPC)[7] (E). $^3J_{HNHA}$ coupling constants of the 15-mer in the absence (red) and presence of 300 mM NaCl (black).

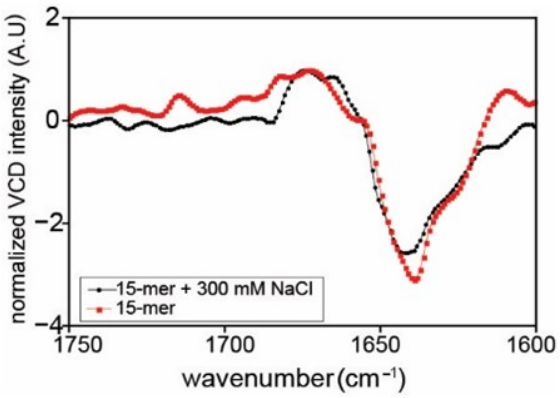

Fig. S5 Normalized VCD intensities of the 15-mer in the absence (red) and presence of 300 mM NaCl (black).

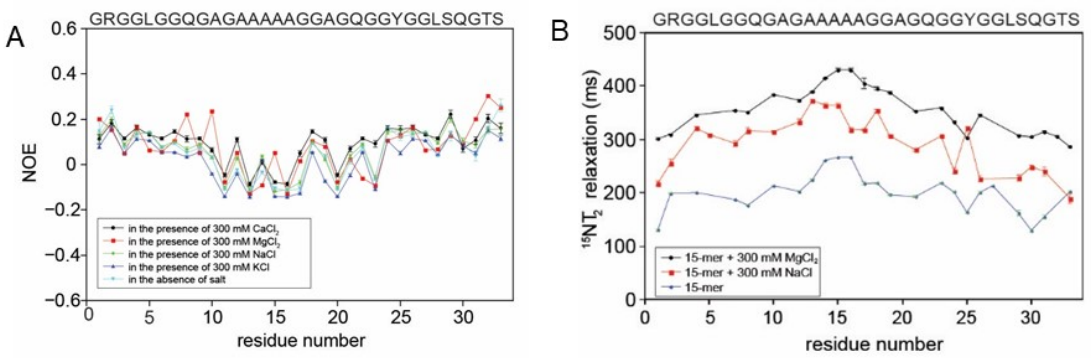

Fig. S6 Effect of chaotropic ions on the dynamics of the repetitive domain (15-mer). (A). The effect of chaotropic ions on the $\{^{1}H\}$-^{15}N heteronuclear NOE of the 15-mer in the absence of salt (cyan), in the presence of 300 mM KCl (dark blue), in the presence of 300 mM NaCl (green), in the presence of 300 mM $MgCl_2$ (red) and in the presence of 300 mM $CaCl_2$ (black). Based on these results, chaotropic ions do not affect the local dynamics of the 15-mer (B). The effect of chaotropic ions on the ^{15}N T_2 relaxation of the 15-mer in the absence of salt (blue), in the presence of 300 mM NaCl (red) and in the presence of 300 mM $MgCl_2$ (black). These $^{15}NT_2$ relaxation data suggest that chaotropic ions affect the dynamics of the repetitive domain on a slow time scale (ns time scale). The fact that ^{15}N T_2 relaxation increases in the presence of chaotropic ions might be explained based on 2 reasons: (1) chaotropic ions might suppress conformational exchange and (2) chaotropic ions might prevent intermolecular interactions. A higher ionic strength (Mg^{2+}) causes a greater effect on the $^{15}NT_2$ relaxation of the 15-mer. These data suggest that a higher ionic strength salt might prevent intermolecular interactions more efficiently, causing the repetitive domain to remain monomeric.

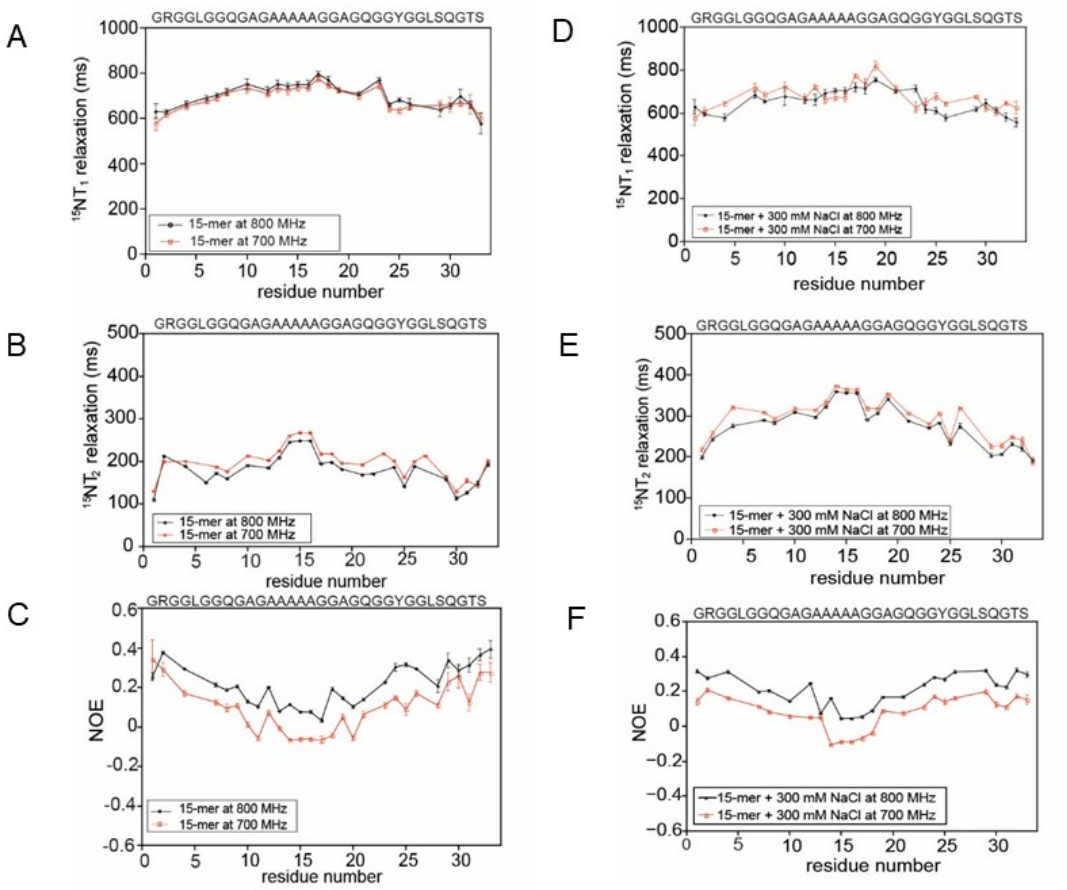

Fig. S7 Complete dynamics measurements of the 15-mer in the presence and absence of 300 mM NaCl. (A) $^{15}NT_1$ relaxation of the 15-mer. (B) $^{15}NT_2$ relaxation of the 15-mer. (C) {^{1}H}-^{15}N Heteronuclear NOE of the 15-mer. (D) $^{15}NT_1$ relaxation of the 15-mer in the presence of 300 mM NaCl. (E) $^{15}NT_2$ relaxation of the 15-mer in the presence of 300 mM NaCl. (F) {^{1}H}-^{15}N Heteronuclear NOEs of the 15-mer in the presence of 300 mM NaCl. All measurements were performed at 15°C.

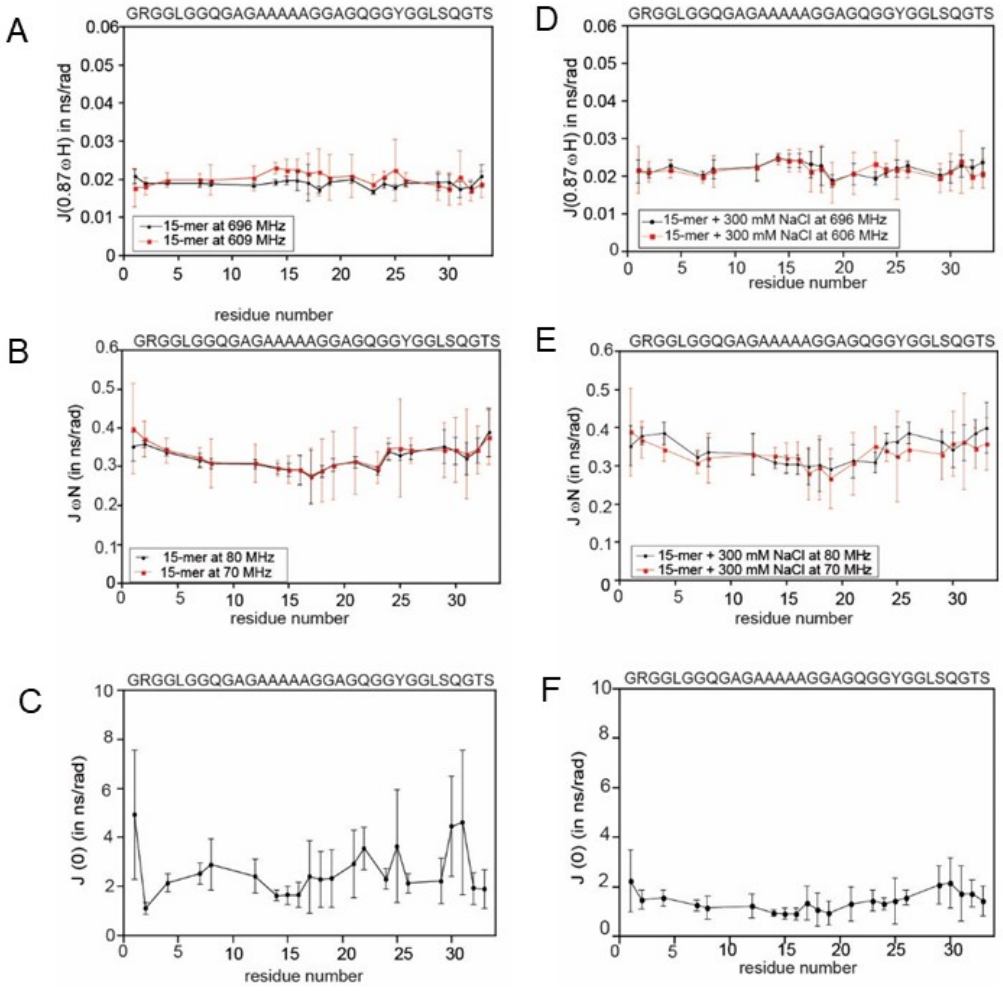

Fig. S8 Spectral density analysis of the 15-mer in the absence and presence of 300 mM NaCl. (A) J(696 MHz) (black) and J(609 MHz) red of the 15-mer. (B) J(80 MHz) (black) and J(70 MHz) (red) of the 15-mer. (C) J(0) of the 15-mer. (D) J (696 MHz) (black) and J(609 MHz) (red) of the 15-mer in the presence of 300 mM NaCl. (E) J(80 MHz) black and J(70 MHz) red of the 15-mer in the presence of 300 mM NaCl. (F) J(0) of the 15-mer in the presence of 300 mM NaCl.

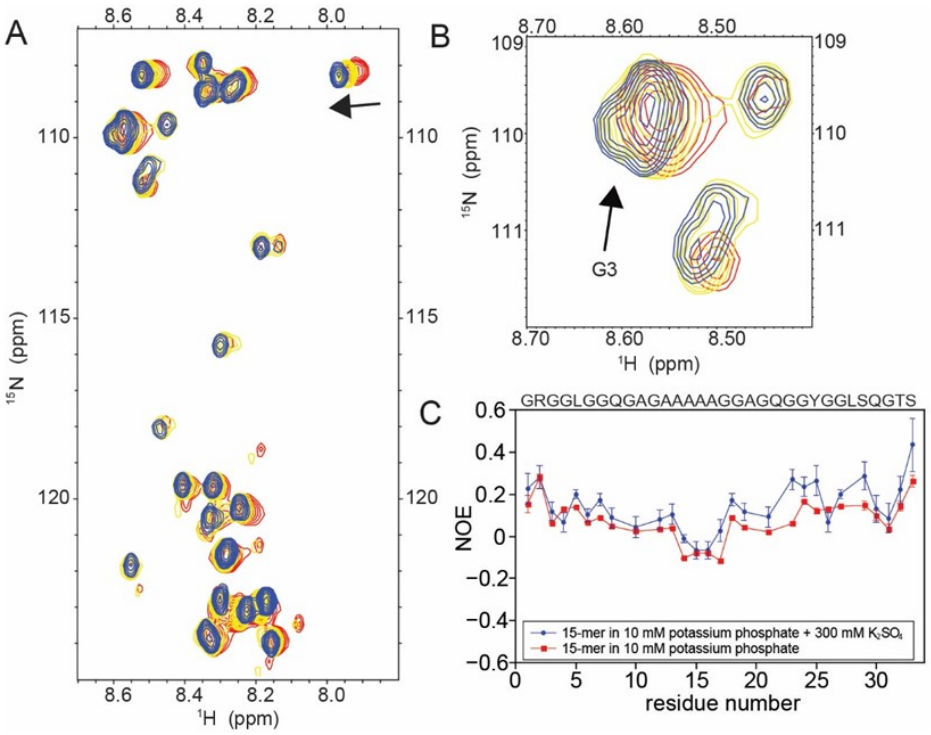

Fig. S9 Effect of kosmotropic ions (SO_4^{2-}) on the conformation and dynamics of the repetitive domain (15-mer). (A) 2D ^{1}H-^{15}N HSQC spectra of the 15-mer in different potassium sulfate concentrations. The spectra of the 15-mer acquired in 0 mM, 100 mM, and 300 mM potassium sulfate are shown in red, yellow and blue, respectively. The arrow indicates the glycine signals that are shifted downfield. (B) Expansion of the ^{1}H-^{15}N HSQC spectra of the glycine-rich region of the 15-mer. In the presence of 300 mM (blue) potassium sulfate, broadening of the proton signals was observed in the glycine-rich region, and the proton signals of residue G3 were shifted downfield and did not overlap with other glycine signals, suggesting that kosmotropic ions (SO_4^{2-}) promote hydrogen bonding interactions in this region. (C) {^{1}H}-^{15}N heteronuclear NOE of the 15-mer in the absence (red) and presence of 300 mM potassium sulfate (blue). In the presence of 300 mM potassium phosphate, the NOE values of the 15-mer were slightly increased, particularly in the glycine-rich region. Overlapping signals were not considered in the {^{1}H}-^{15}N heteronuclear NOE analysis.

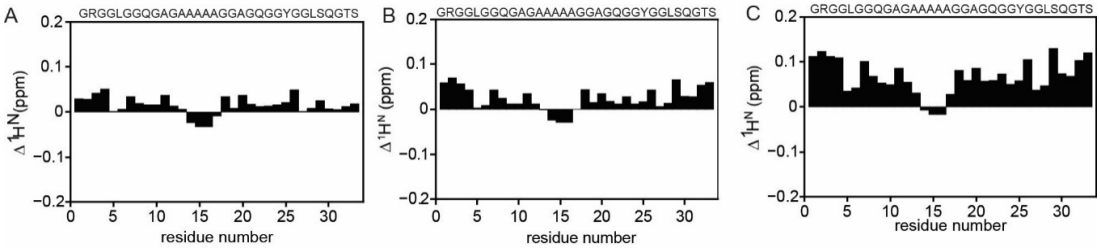

Fig. S10 Effect of kosmotropic ions on the amide proton of the repetitive domain. (A) The effect of 300 mM potassium sulfate on the amide proton of the repetitive domain as a function of residue number. The delta of the amide proton (Δ^1H^N) is calculated by subtracting the amide proton of the 15-mer in the presence and absence of 300 mM potassium sulfate. (B) The effect of 300 mM potassium phosphate on the amide protons as a function of residue number. The delta of the amide proton (Δ^1H^N) is calculated by subtracting the amide proton of the 15-mer in the presence and absence of 300 mM potassium phosphate. (C) The effect of 600 mM potassium phosphate on the amide protons as a function of residue number. The delta of the amide proton (Δ^1H^N) is calculated by subtracting the amide proton of the 15-mer in the presence and absence of 600 mM potassium phosphate. All experiments were performed at 15°C. The positive delta amide proton values indicate that the amide protons were shifted downfield.

Fig. S11 Higher phosphate concentrations (≥ 600 mM) lead to precipitation of the 15-mer.

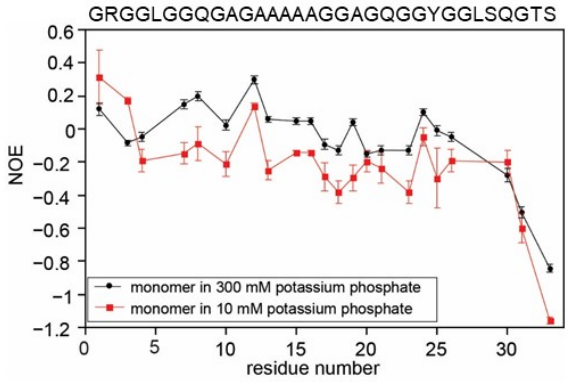

Fig. S12 Effect of 300 mM potassium phosphate on the dynamics of the monomer. The $\{^{1}H\}$-^{15}N heteronuclear NOEs of the monomer in the presence of 10 mM (red) and 300 mM potassium phosphate (black) were plotted as a function of residue number. The higher NOE values of the monomer in the presence of 300 mM potassium phosphate suggest that a higher phosphate concentration reduces the local flexibility of the monomer due to intermolecular interactions.

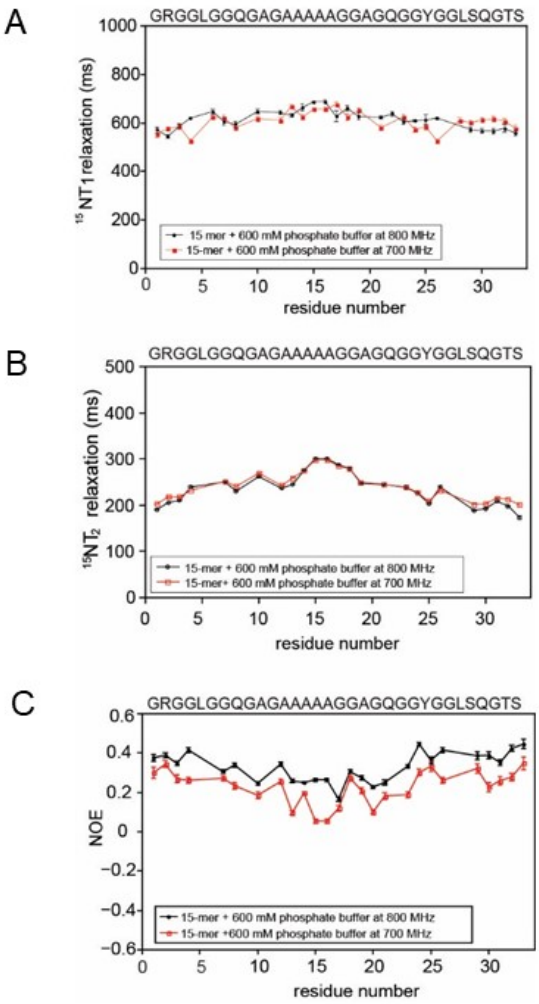

Fig. S13 Complete dynamics measurements of the 15-mer in the presence of 600 mM potassium phosphate. (A) $^{15}NT_1$ relaxation of the 15-mer in the presence of 600 mM potassium phosphate, pH 7. (B) $^{15}NT_2$ relaxation of the 15-mer in the presence of 600 mM potassium phosphate, pH 7. (C) {^{1}H}-^{15}N Heteronuclear NOE of the 15-mer in the presence of 600 mM potassium phosphate. All spectra were acquired at 15°C.

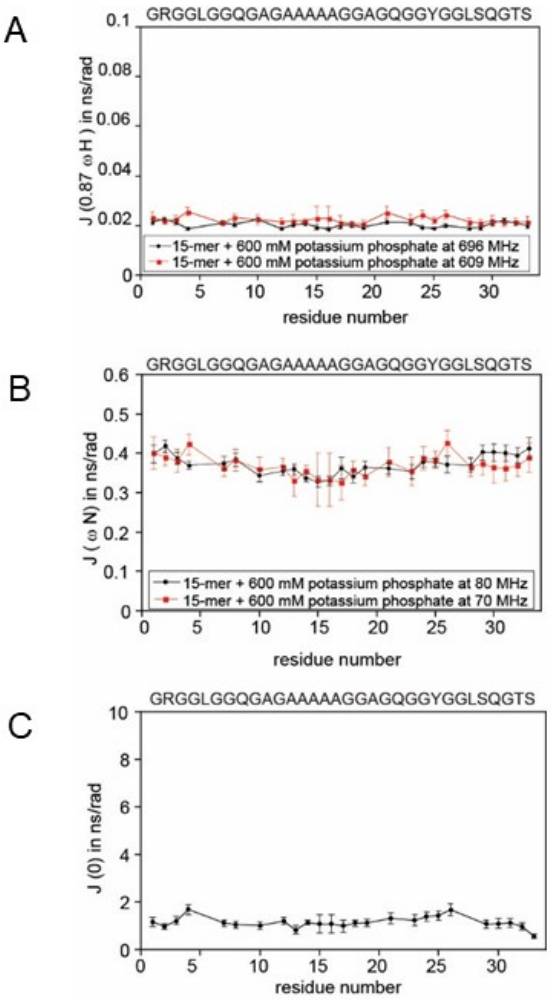

Fig. S14 Spectral density of the 15-mer in the presence of 600 mM potassium phosphate. (A) J(696 MHz) (black) and J(609 MHz) red of the 15-mer in the presence of 600 mM potassium phosphate. (B) J(80 MHz) (black) and J(70 MHz) (red) of the 15-mer in the presence of 600 mM potassium phosphate. (C) J(0) of the 15-mer in the presence of 600 mM potassium phosphate.

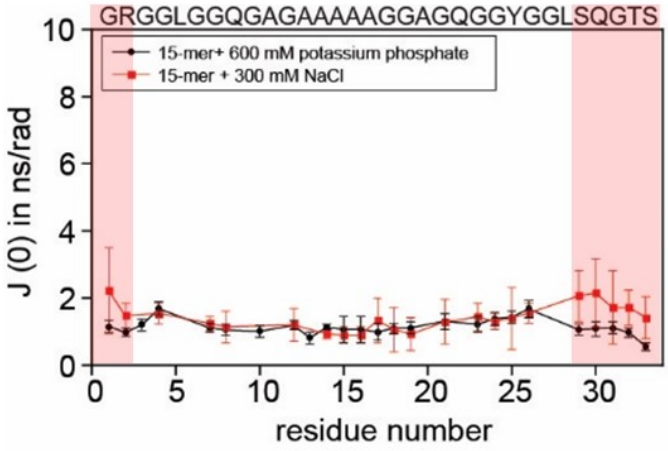

Fig. S15 Comparison of J(0) values of the 15-mer in the presence of 600 mM potassium phosphate (black) and in the presence of 300 mM NaCl (red). Most residues have similar J(0) values except the SQGTSGR residues (red shadow). The smaller J(0) values of the 15-mer in the presence of 600 mM potassium phosphate suggest that this region is more likely to contain a turn. G3 is excluded in the J(0) analysis of the 15-mer in the presence of 300 mM NaCl because it overlaps with other glycine residues. Other overlapping signals were removed from the plot.

References

1 J. T. Prince, K. P. McGrath, C. M. DiGirolamo and D. L. Kaplan, *Biochemistry*, 1995, **34**, 10879–10885.
2 K. Numata, B. Subramanian, H. A. Currie and D. L. Kaplan, *Biomaterials*, 2009, **30**, 5775–5784.
3 N. A. Oktaviani, A. Matsugami, A. D. Malay, F. Hayashi, D. L. Kaplan and K. Numata, *Nat. Commun.*, 2018, **9**, 2121.
4 F. Delaglio, S. Grzesiek, G. W. Vuister, G. Zhu, J. Pfeifer and A. Bax, *J. Biomol. NMR*, 1995, **6**, 277–293.
5 W. Lee, M. Tonelli and J. L. Markley, *Bioinforma. Oxf. Engl.* 2015, **31**, 1325–1327.
6 J. L. Markley, A. Bax, Y. Arata, C. W. Hilbers, R. Kaptein, B. D. Sykes, P. E. Wright and K. Wüthrich, *J. Biomol. NMR*, 1998, **12**, 1–23.
7 K. Tamiola and F. A. A. Mulder, *Biochem. Soc. Trans.*, 2012, **40**, 1014–1020.
8 G. W. Vuister and A. Bax, *J. Am. Chem. Soc.*, 1993, **115**, 7772–7777.
9 T. Yuwen and N. R. Skrynnikov, *J. Magn. Reson. San Diego Calif 1997*, 2014, **241**, 155–169.
10 N. A. Farrow, R. Muhandiram, A. U. Singer, S. M. Pascal, C. M. Kay, G. Gish, S. E. Shoelson, T. Pawson, J. D. Forman-Kay and L. E. Kay, *Biochemistry*, 1994, **33**, 5984–6003.
11 N. A. Farrow, O. Zhang, A. Szabo, D. A. Torchia and L. E. Kay, *J. Biomol. NMR*, 1995, **6**, 153–162.